

The Possibility of Chemically Inert, Graphene-Based All-Carbon Electronic Devices with 0.8 eV Gap

Jing Shan Qi,^{†,‡} Jian Yu Huang,^{§,*} Ji Feng,[†] Da Ning Shi,[‡] and Ju Li^{†,*}

[†]Department of Materials Science and Engineering, University of Pennsylvania, Philadelphia, Pennsylvania 19104, United States ,

[‡]Department of Applied Physics, Nanjing University of Aeronautics and Astronautics, Nanjing 210016, China, and [§]Center for Integrated Nanotechnologies, Sandia National Laboratories, Albuquerque, New Mexico 87185, United States

Graphene, a two-dimensional (2D) allotrope of carbon, has attracted a lot of interest recently for its unique properties.^{1,2} Flat graphene is a zero-gap semimetal with light-like dispersion of the electronic energy E_k near the Fermi level, which implies that the electronic effective mass is zero and the system can be described by a relativistic Dirac equation.² Carbon nanotubes,³ a one-dimensional (1D) allotrope of carbon with translational periodicity along the tube axis, are obtained by rolling graphene along a certain direction by 2π . The electronic and transport properties of carbon nanotubes crucially depend on the diameter and chirality.^{4–6} Both flat graphene (monolayer^{7,8} or bilayer^{9,10} graphene) and curved graphene (e.g., single-wall carbon nanotubes^{11,12}) are being actively explored as candidate materials for room-temperature electronic devices. To give a large on–off ratio in the current, required for logic functions, it is necessary for these carbon structures to possess a significant energy gap in the electron transmission spectrum. The ballpark value for this gap, E_g , should be around that of silicon, 1.1 eV.

Semiconducting single-wall carbon nanotubes (SWCN) with appropriate chirality and diameter have E_g of this magnitude^{4,6} and indeed may show superior performance to silicon-based devices at individual device-element levels.¹² The main problem, however, is the assembly process and device reproducibility. Carbon nanotubes are structurally polydisperse, as SWCNs with different chirality and diameter are nearly degenerate in energy and often coexist. With the usual paradigm of using SWCNs, after growing the nanotubes somewhere else, one needs to take them out, sort them,¹³ cut, manipulate, and orient one on

ABSTRACT Graphene is an interesting electronic material. However, flat monolayer graphene does not have significant gap in the electronic density of states, required for a large on–off ratio in logic applications. We propose here a novel device architecture, composed of self-folded carbon nanotube–graphene hybrids, which have been recently observed experimentally in Joule-heated graphene. These experiments demonstrated the feasibility of cutting, folding, and welding few-layer graphene *in situ* to form all-carbon nanostructures with complex topologies. The electronic gap of self-folded nanotubes can be combined with the semimetallicity of graphene electrodes to form a “metal–semiconductor–metal” junction. By *ab initio* calculations we demonstrate large energy gaps in the transmission spectra of such junctions, which preserve the intrinsic transport characteristics of the semiconducting nanotubes despite topologically necessary disinclinations at the flat graphene–curved nanotube interface. These all-carbon devices are proposed to be constructed by contact probe cutting and high-temperature annealing and, if produced, would be chemically stable at room temperature under normal gas environments.

KEYWORDS: self-folding · graphene · nanotube · half-nanotube · bilayer edge · hybrid device

a substrate, and then interface with a metal electrode material, using for instance ion beam deposition. This device assembly process is time-consuming, not scalable, and far from automated, and the device performance often has large scatter due to uncertainties in the nanotube type, as well as metal–carbon atomic contact conditions at the electrode interface. With low work-function metal electrode materials, experiments¹⁴ have shown the existence of a Schottky contact barrier at the SWCN–metal interface, which dominates the device behavior and makes the performance very sensitive to the contact conditions.¹⁵ Because it is difficult to construct device junctions with atomically controlled interfaces, different samples produced by nominally the same process would have different detailed atomic geometries and metal–carbon bonding arrangements, giving huge scatter in the device characteristics. Using high work-function metal electrode materials, for example, Pd,

* Address correspondence to
jhuang@sandia.gov;
liju@seas.upenn.edu.

Received for review September 7, 2010
and accepted April 1, 2011.

Published online April 01, 2011
10.1021/nn102322s

© 2011 American Chemical Society

it is possible to achieve Ohmic contact,¹⁶ with somewhat reduced contact sensitivity, but the sensitivity is still nonzero and indeed quite large.^{17,18} All these are exacerbated by the promiscuous nature of metallic bonding and the fact that these metal–carbon interfaces must be incoherent, which makes the contact ill-controlled and polydisperse at the atomic level.

Compared to conventional carbon nanotube-based devices, flat graphene is attractive because of large-area production^{19,20} and scalable processing by tried-and-true top-down approaches inherited from the semiconductor industry, such as patterning and electron lithography. However, monolayer graphene is a semimetal with $E_g = 0$ (therefore used as transparent electrode material^{19,20}). A band gap can open up when graphene nanoribbons (GNRs) with two parallel hydrogen passivated monolayer edges (MLEs) are created on monolayer graphene, due to quantum confinement effect,^{7,21} and the band gap of GNRs depends sensitively on the crystallographic orientation of their edges and width.^{21,22} The problem here is that MLEs are atomically rough^{23,24} and chemically reactive: the C–H bonds can be replaced or modified by other volatile adsorbates/adsorbates, depending on the gas environment, that change the characteristics of the GNR device. The influence of edge molecule adsorption and defects on electronic properties of GNR has been extensively studied in recent years,^{25–27} highlighting this problem. In addition, MLE also has edge stress that tends to cause warping of the nanoribbon,²⁸ which further increases the structural uncertainty. For these and other reasons, bilayer graphene^{9,10,29,30} and bilayer graphene edges (BLEs)^{31–33} may provide a more promising platform for logic applications. Among other things, the closed bilayer edges (*aka* half-nanotubes) are atomically straight and chemically inert.^{31–33} They are built out of pure carbon atoms (no H, O, N, ..., volatiles involved), are completely sp^2 bonded without dangling bonds, and are structurally highly monodisperse for geometric reasons.^{24,33} In addition, bilayer graphene can also manifest a band gap up to 0.25 eV when an external electric field is applied in the perpendicular direction,^{9,10} although this is still somewhat small for room-temperature applications (an on–off ratio of 100 was achieved experimentally¹⁰).

On the basis of the separate advantages of carbon nanotubes and graphene, in this paper we propose a novel device architecture, composed of carbon nanotube–graphene hybrids, which have been recently observed experimentally in Joule-heated graphene. The electronic band gap of self-folded nanotubes can be combined with the semimetallicity of graphene electrodes to form a “metal–semiconductor–metal” junction. By molecular dynamics simulations we show a pathway for constructing an all-carbon device starting from a perfectly flat bilayer graphene sheet

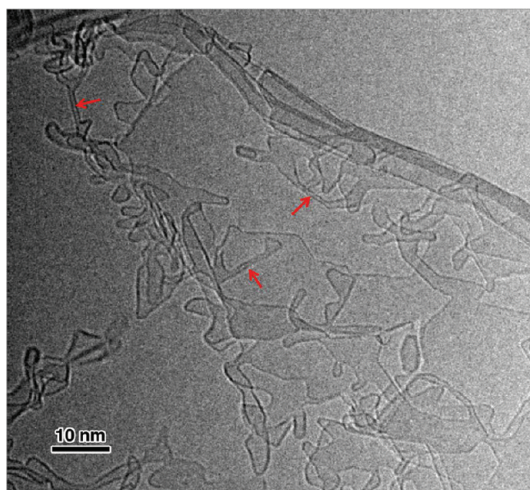


Figure 1. High-resolution TEM image of single-walled nanotubes that bridge few-layer graphene. The red arrows point out carbon nanotubes.

and confirm its stability. By *ab initio* transport calculations we demonstrate a large energy gap in the transmission spectrum of such junctions. These all-carbon devices are proposed to be constructed by self-folding after contact-probe cutting and high-temperature annealing and, if produced, would be chemically stable at room temperature under normal gas environments. In the following, we will demonstrate those aspects in detail.

RESULTS AND DISCUSSION

Concepts and Advantages of Device Design. We propose a hybrid nanotube–graphene device design that has the best of both worlds: the large gap (near 1 eV) of semiconducting carbon nanotubes and the processability and semimetallicity of bilayer graphene, with a coherent all-carbon interface in between. Our design is inspired by recent *in situ* experiments of Joule-heating few-layer graphene inside a transmission electron microscope (TEM), where a similar kind of all-carbon nanostructures has been observed,^{24,32} demonstrating their stability. Figure 1 shows a TEM micrograph of single-wall carbon nanotubes that connect to BLE^{31–33} and bridge a few layers of flat graphene. See also Movies M1 and M2 in the Supporting Information, the real-time assembly dynamics of all-carbon junctions in high-resolution TEM. Figure 1 and Movies M1 and M2 are here invoked to reaffirm and strengthen the experimental observations of our previous paper.³² The main point of ref 32 as well as ref 31 is that all the edges one sees in Figure 1 are self-folded bilayer edges with nanoscopic curvature rather than flat monolayer edges. If one accepts this basic premise, then the thin rod-like objects one sees in Figure 1 (see also Figure 5 of ref 32) can only be single-walled carbon nanotubes. This is because the rod diameters are visually measured to be around 1 nm (0.7–0.8 nm in high-resolution Figure 5 of ref 32). Many commonly observed SWCNs have diameters

in this range. But it cannot be even a double-walled carbon nanotube (DWCN), whose usual diameter is around 1.5 nm. Also note how straight the thin rods tend to be. This is because nearly perfect SWCNs are formed by self-folding and thermal annealing, with few defects. These self-folded nanostructures with contacts already in place (the mother graphene) can have very useful transport properties, as we will show.

It is worth noting that our device design differs from traditional nanotube-based devices in two important ways. First, it is made entirely out of carbon, all sp^2 -bonded carbon in fact. No metallic elements are necessary as electrodes, since flat graphene is already a reasonable electrode material.^{19,20} The problem of graphene edge states is resolved by self-wrapping and self-passivation to form curved SWCNs and BLEs. No H, O, N, ..., volatiles are involved (the experiments^{24,32} were performed in high vacuum). This coherent junction of flat carbon and curved carbon³² possesses similar physical and chemical inertness to carbon nanotubes.

Second, the way our devices are assembled (“self-folding” approach) differs fundamentally from the traditional approaches of growing carbon nanotubes somewhere (for instance arc-discharge or chemical-vapor-deposition chamber) and then using them somewhere else. The self-folded structures were created by cutting graphene,^{24,32} which then curls up due to edge stress and thermal fluctuations and welds together, *while maintaining connection to the mother graphene*. Therefore no subsequent handling or electrification is necessary. The biggest obstacle to exploiting the extraordinary properties of nanotubes is their handling and assembly. Our *in situ* assembly approach is possible only in two-dimensional layered material where bending is easy, analogous to plumbers working on sheet metals. Consequently, SWCN can be fabricated directly into device structures and even integrated circuits by a process of patterning few-layer graphene and annealing.

Before delving into theoretical details of the device design, we remark on two points concerning practical processing. First, although previously for fundamental studies³² uniform Joule-heating^{24,32} was used to cut holes in graphene, Joule-heating is not a good way to do practical patterning because it is too delocalized in a very high thermal conductivity material. Electron lithography⁷ or contact probes³⁴ would be needed for precise incision of graphene. Second, medium- to high-temperature annealing is absolutely essential. It was found from the previous experiments that without annealing the graphene would gradually turn amorphous due to defects induced by 300 keV electron beam damage in the TEM. With Joule-heating^{24,32} turned on, however, the graphene stays highly crystalline, demonstrating that most defects can be effectively

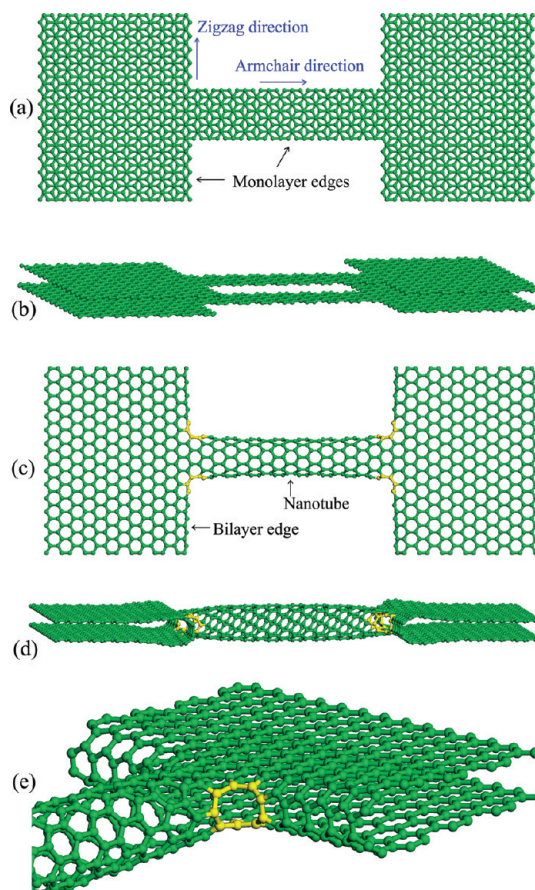


Figure 2. Top view (a) and side view (b) of the initial structure constructed by cutting off two rectangular fragments along zigzag and armchair directions (indicated by blue arrows) from a BLG sheet. Top view (c) and side view (d) of the final structure after annealing at 1500 K in MD simulation for 2 ns. (e) Enlarged view of the part near the corner. Nonagon rings in the corners are indicated by yellow atoms.

annealed out. The temperature involved in those experiments could be as high as 2000 K. Since we want a coherent interface between flat carbon and curved carbon, the amount of defects should be minimized, and thermal annealing is a requisite step. We note here, however, that there are two defect populations in the system: the so-called “intrinsic” (*aka* topologically necessary) *versus* “extrinsic” (*aka* statistically stored) defects, with the distinction that the extrinsic defects can be effectively annealed out by design, but the intrinsic defects (like the 12 pentagons in C_{60}) can never be, due to the geometric requirement of the nanojunction. This is because in order to accommodate the curvature change from flat to curved graphene, a certain number of *topologically necessary* disclination defects (see for example the four nonagons in Figure 2) must be injected at the flat graphene–curved nanotube interface, which necessarily disrupts the perfect hexagonal bonding network. A major result of our work is to demonstrate that the electronic transport characteristics of the nanotube are preserved

despite the topologically necessary intrinsic defects at the graphene–nanotube interface.

Molecular Dynamics (MD) Simulations of Hybrid Device Fabrication. In the following MD simulations, we show a pathway for constructing an all-carbon device starting from a perfectly flat bilayer graphene (BLG) sheet. Figure 2a and b shows the top and side view of the initial structure constructed by cutting off rectangular areas along zigzag and armchair directions from a BLG sheet, respectively. The middle narrow ribbon is a pristine bilayer graphene nanoribbon with unpassivated armchair MLEs. Previous *ab initio* calculation indicated that the armchair (8,8) SWCN can be formed from two bare graphene nanoribbons with zigzag-shaped edges without any significant activation barrier, while the formation of a zigzag (10,0) SWCN from two bare graphene nanoribbons with armchair-shaped edges has activation barriers of several tenths of an electronvolt.³⁵ In our initial structures there are two types of unsaturated monolayer edges, armchair and zigzag, which need to overcome activation energy barriers due to bending to form closed edges. Our MD simulations show that at $T = 300$ K the closed edges cannot be formed in 2 ns total simulation time. On the other hand, by annealing at elevated temperatures, we can overcome the bending energy barrier to form closed edges. When the temperature is increased gradually from 300 to 1500 K in a 2 ns simulation run, the closed edges are formed. Top and side views of the final system configuration are shown in Figure 2c and d, respectively. All the edges of BLG are closed, and the middle part (as a channel in the transport model) of the system becomes a zigzag SWCN.

Here we should point out that we also can obtain armchair SWCNs if we cut off rectangle areas to make the initial middle bilayer nanoribbon with zigzag edges. So by controlling the cutting direction we can control the type of SWCN, armchair or zigzag type. Because all armchair SWCNs are metallic, in the rest of this paper we will focus our discussion on semiconducting zigzag SWCNs for illustrating the intrinsic semiconducting transport properties for field-effect transistor (FET) application.

From MD simulation we find that the junction between SWCN and BLG is atomically smooth and the edges of BLG are atomically smooth curved BLEs (*aka* half-nanotubes, due to π rotation of graphene³³ instead of 2π rotation in a full nanotube), which have been discovered experimentally by high-resolution TEM^{24,31,32} recently. This indicates that the BLEs are much more stable than MLEs, because forming a closed edge (or nanotube) through eliminating dangling bonds is more energetically favorable than any type of MLEs with dangling bonds, under high-vacuum conditions. Our first-principles calculation also shows that a closed bilayer edge is energetically lower by ~ 1 eV/Å than two monolayer edges, indicating the

results from our MD simulation are reasonable. Another observation is that the stacking between two graphene layers changes from initial AB type to final AA type. This phenomenon has been observed experimentally from detailed TEM³¹ and extensively discussed based on geometric and energetic grounds.^{24,33}

In the current system all carbon atoms are fully sp^2 -coordinated, although there are nonhexagon rings, which are the nonagon rings indicated by yellow atoms in four corners in junctions between BLG and SWCN in the structure of Figure 2, due to the transition from the armchair direction (SWCN) to the zigzag direction (BLEs). In contrast, unpassivated MLEs always have unsaturated carbon atoms (dangling bonds), which are chemically reactive, even in the reconstructed zigzag and armchair MLEs.³⁶ On the other hand, if the edge has been passivated in a gaseous environment, the atomic structure of the MLEs may be rugged, and the chemical nature might be difficult to ascertain (N, O, H, ..., volatiles). It is well known that the transport properties of graphene are sensitive to edge terminations² in the case of MLEs. The influence of gas molecule adsorption and edge defects on electronic properties of nanoribbons has been extensively studied in recent years.^{25–27} These disadvantages are all from the existence of monolayer edges of graphene nanoribbons. In contrast, the closed BLEs are more strongly crystallographically faceted than MLEs.^{24,33} When two MLEs react to form a more stable BLE, the newly formed BLE tends to be atomically sharp and strongly faceted into zigzag and armchair inclinations.^{31,32} They are built out of pure carbon atoms (no H, O, N, ..., volatiles involved) and are completely sp^2 bonded without dangling bonds. The structural certainty and chemical inertness under normal gas environment are great advantages for BLEs and SWNTs compared to MLE nanoribbons. They provide us a potential avenue to make graphene-based nanodevices with controllable electronic properties.

We also evaluate the maximum width of the middle channel, which can become a SWCN, not a BLG nanoribbon enclosed by two BLEs (collapsed SWCN). MD simulation shows that the channel can become a *bona fide* SWCN when the width of the channel is less than 2.5 nm. When the width is larger than 2.5 nm, the SWCN collapses into two parallel BLEs, due to van der Waals adhesion between the top and bottom layers. From the view of application as semiconductor devices we hope that the energy gap of SWCNs is no less than 0.7 eV. This requires that the diameters of SWCNs are about 0.7–1.1 nm. In this range of diameters, our MD simulations show that SWCNs can be formed spontaneously from bilayer graphene nanoribbons by annealing at high temperature.

Experimentally this novel structure may be fabricated by AFM cutting, STM cutting, or catalyst particle cutting³⁷ for making electronic circuits. Well-defined

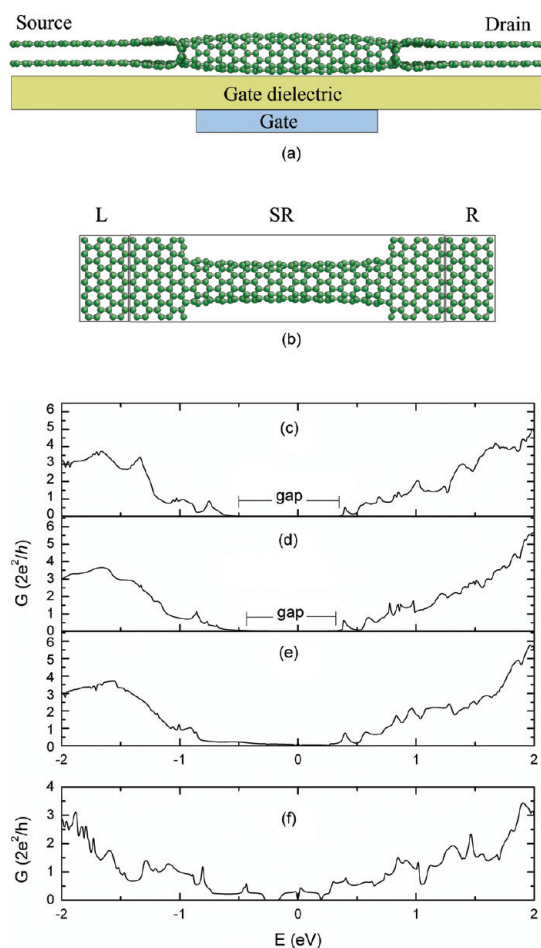


Figure 3. (a) Side view of a FET device model. (b) Two-probe computational model used in transport calculation, where left (L) and right (R) leads are semi-infinite BLGs and the scattering region (SR) is a BLG–SWCN junction. Electrical conductance of the BLG–SWCN junction made with a 3.6 nm (c), 2.8 nm (d), and 1.8 nm (e) long semiconducting (8, 0) SWCN as a channel connected to two BLGs with curved edges. (f) Electrical conductance of a BLG–SWCN junction made with a 3.6 nm long metallic (6, 0) SWCN as a channel connected to two BLGs with curved edges.

shapes can be cut on a BLG sheet, as shown in Figure 2. Once cut, the sheets can be annealed at high temperature, and then the closed edges of the BLG sheet can be formed by self-folding. Those structures are continuous and all sp^2 covalently bonded; thus contact resistances would be minimized, as shown in the next section.

Quantum Transport Properties. In the following, we demonstrate the intrinsic semiconducting transport behaviors of these device models from first-principles calculations. A FET device model constructed from SWCN and BLG is illustrated in Figure 3a. Furthermore we performed quantum transport calculations of a BLG–SWCN coherent junction (analogous to the concept of coherent or semicoherent interfaces in materials science language) by the density functional theory (DFT) and nonequilibrium Green's function formalism (NEGF). The transport behaviors of the BLG–SWCN

junction are calculated with a two-probe model shown in Figure 3b. Figure 3c, d, and e shows the electrical conductance (G) of the BLG–SWCN junction made with 3.6, 2.8, and 1.8 nm long semiconducting (8, 0) SWCNs as channels connected to two BLGs with curved edges, respectively. Electrical conductance in Figure 3c and d obviously shows the semiconducting behavior with about 0.8 eV transport gap, which is close to the band gap of infinitely long (8, 0) SWCNs (0.9 eV).

We should also point out that the length of the SWCN also affects the transport properties of the BLG–SWCN junctions. When the SWCN is too short, tunneling can obliterate the semiconducting behavior. As an estimate, Figure 3e shows the electrical conductance of the BLG–SWCN junction with a 1.8 nm long (8, 0) SWCN as a channel. The transport of this shorter BLG–SWCN junction shows metallic behavior, although conductance is small near the Fermi energy. This indicates that the shorter SWCN can result in current leakage. This can be understood in terms of a quantum tunneling mechanism. There is an energy gap near the Fermi energy for a semiconducting SWCN, which acts as a barrier against carrier transmission. Because tunneling probability across a barrier decreases exponentially with the width of the barrier, the small width of the barrier can cause a significant increase of tunneling probability. Consequently, in device design the semiconducting SWCN should be long enough to suppress the tunneling current. In our case, at least 2.8 nm lengths are required to avoid this effect and get a semiconducting transport behavior.

In order to further prove that the semiconducting transport behavior of this system arises intrinsically from the semiconducting character of the (8, 0) SWCN rather than from the effect of contact between BLG and SWCN, we also calculated the transmission spectrum of the BLG–SWCN junction with a 3.6 nm long metallic (6, 0) SWCN as a channel. Results are shown in Figure 3f. The BLG–SWCN junction with a (6, 0) SWCN as channel shows metallic behavior, as expected. Therefore we can conclude that the transport behavior of the junction depends on the intrinsic behavior of the SWCN, and the effect of contact on the transport properties is negligible. This is because there is an atomically coherent interface between the SWCN and BLG, besides the four nonagon rings, which are geometrically necessary disclinations to accommodate the curvature change.

Lastly we briefly discuss the impact of possible extrinsic defects. If the initial edges are not perfectly cut, closed BLEs and SWCTs can still be formed automatically by self-folding, but with some additional extrinsic defect(s) in the nanojunction. As shown in Figure 4a, b, and c, the self-folded nanojunction contains an extrinsic defect composed of two pentagons and one octagon if two adjacent atoms at an armchair edge are removed in the initial structure, like a

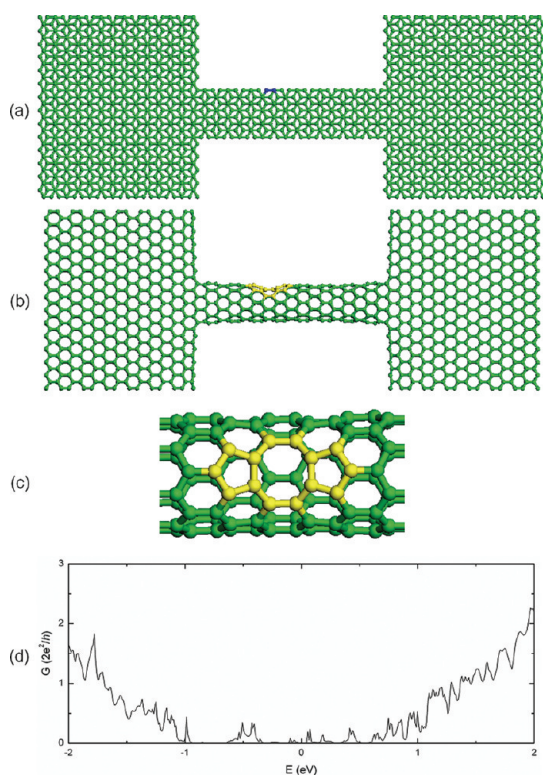


Figure 4. Top view of the initial structure (a) with two removed adjacent atoms (highlighted by blue atoms) at an armchair edge and the final structure (b) after annealing at 1500 K in a MD simulation for 2 ns with a defect composed of two pentagons and one octagon (highlighted by yellow atoms). (c) Enlarged view of the structure near the defect. (d) Electrical conductance of the BLG–SWCN junction made with a 3.6 nm long semiconducting (8, 0) SWCN with a defect composed of two pentagons and one octagon.

divacancy in the carbon nanotube.^{38,39} Because the parameter space of possible extrinsic defect configurations is large, we cannot exhaustively study extrinsic defects here and just show one example to illustrate the effects. In Figure 4d we plot the electrical conductance of the BLG–SWCN junction with one extrinsic and four intrinsic defects. By comparing Figure 4d with

Figure 3c, we see that the extrinsic defect introduces some states in the transport gap but otherwise does not change the main gap feature, akin to the conclusion drawn by previous work about SWCNs with point defects.^{40–42} Furthermore, because the self-folding paradigm is a high-temperature process, the extrinsic defects have a much higher likelihood of being annealed out. It was found from the previous experiments that without annealing the graphene would gradually turn amorphous due to defects induced by 300 keV electron beam damage in the TEM. With Joule-heating^{24,32} turned on, however, the graphene stays highly crystalline, demonstrating that the extrinsic defects can indeed be effectively annealed out at temperatures around 1500–2000 K.

CONCLUSION

In conclusion, we illustrate architectural designs of all-carbon electronic devices based on BLG and SWCN by MD simulations and demonstrate the intrinsic semiconducting transport behaviors of these device models from first-principles calculations. The junction between BLG and SWCN has a coherent atomic interface and the whole device consists of full- sp^2 bonding carbon atoms without dangling bonds or exotic atoms, so that the device is very stable against temperature and environment. There are two key potential advantages in our SWCN–BLG design and the self-folding process. First, the junction between BLG and SWCN has a smooth atomic interface with minimum contact resistance. Generally there exists a large contact resistance or even Schottky barrier between the metal electrodes and SWCN due to a very small contact area and incoherent metal–carbon interface.^{17,18} Second, the whole device consists of a full- sp^2 bonded net of carbon atoms without dangling bonds so that the device will be very stable thermally and chemically. This device concept, based on the self-folding we observed experimentally, may lead to a new paradigm for engineering all-carbon integrated circuits in the future.

METHODS

MD simulation is performed for showing how to construct a SWCN–BLG hybrid device from a perfect flat bilayer graphene sheet and demonstrating their stability. The initial structure is constructed by cutting off rectangular areas along the zigzag and armchair directions from a BLG sheet, respectively. This initial structure is modeled as a two-dimensional periodic structure. Interaction between carbon atoms is described by the adaptive intermolecular reactive empirical bond order (AREBO) potential,⁴³ where a parameterized bond order function is used to introduce many-body effects and chemical bonding. For observing the formation of hybrid structures, first we performed MD simulations at $T = 300$ K for 2 ns total simulation time, and then we gradually increased the temperature from 300 to 1500 K in a 2 ns simulation run.

Quantum transport calculations of the SWCN–BLG coherent junction (analogous to the concept of a coherent or semicoherent interface in materials science language) are performed by using an *ab initio* code, TRANSIESTA,⁴⁴ which is based on a real-space, nonequilibrium Green's function formalism and the density functional theory, as implemented in the SIESTA approach.⁴⁵ In the calculations, structural optimizations were first carried out until atomic forces converged to 0.04 eV/Å. We employ norm-conserving pseudopotentials⁴⁶ and the local-density approximation (LDA).⁴⁷ A real-space grid equivalent to an energy cutoff of 100 Ry is generated to achieve the balance between calculation efficiency and accuracy. The transport behaviors of the BLG–SWCN junction are calculated with a two-probe model shown in Figure 3b, where left and right leads are semi-infinite BLGs and the scattering region is a BLG–SWCN junction. The central scattering region is converged *via* standard

DFT methods. The Kohn–Sham potential outside the scattering region is set to the bulk value of two electrodes, which is determined *via* a separate calculation and shifts rigidly relative to each other by the external bias voltage. The infinite open boundary problem is thereby reduced to a proper, self-consistent calculation of the charge density for the finite sized scattering region.

Acknowledgment. This work was supported by NSF DMR-0520020, Honda Research Institute USA, and AFOSR FA9550-08-1-0325. J.Q. thanks the support by China Scholarship Council and NSFJS No. BK2010499. This work was performed, in part, at the Center for Integrated Nanotechnologies, a U.S. Department of Energy, Office of Basic Energy Sciences, user facility. Sandia National Laboratories is a multiprogram laboratory operated by Sandia Corporation, a wholly owned subsidiary of Lockheed Martin Company, for the U.S. Department of Energy's National Nuclear Security Administration under contract DE-AC04-94AL85000.

Supporting Information Available: Movies M1, M2: *In situ* high-resolution TEM movies showing the self-folded SWCN and graphene interconnected nanostructures formed during Joule-heating of few-layer graphene. The movies were recorded at 2 frames/second and play at 20× speed. This material is available free of charge *via* the Internet at <http://pubs.acs.org>.

REFERENCES AND NOTES

- Geim, A. K. Graphene: Status and Prospects. *Science* **2009**, *324*, 1530–1534.
- Castro Neto, A. H.; Guinea, F.; Peres, N. M. R.; Novoselov, K. S.; Geim, A. K. The Electronic Properties of Graphene. *Rev. Mod. Phys.* **2009**, *81*, 109–162.
- Charlier, J. C.; Blase, X.; Roche, S. Electronic and Transport Properties of Nanotubes. *Rev. Mod. Phys.* **2007**, *79*, 677–732.
- Kane, C. L.; Mele, E. J. Size, Shape, and Low Energy Electronic Structure of Carbon Nanotubes. *Phys. Rev. Lett.* **1997**, *78*, 1932–1935.
- Ouyang, M.; Huang, J. L.; Cheung, C. L.; Lieber, C. M. Energy Gaps in “Metallic” Single-Walled Carbon Nanotubes. *Science* **2001**, *292*, 702–705.
- Weisman, R. B.; Bachilo, S. M. Dependence of Optical Transition Energies on Structure for Single-Walled Carbon Nanotubes in Aqueous Suspension: An Empirical Kataura Plot. *Nano Lett.* **2003**, *3*, 1235–1238.
- Chen, Z. H.; Lin, Y. M.; Rooks, M. J.; Avouris, P. Graphene Nano-Ribbon Electronics. *Phys. E* **2007**, *40*, 228–232.
- Lin, Y. M.; Dimitrakopoulos, C.; Jenkins, K. A.; Farmer, D. B.; Chiu, H. Y.; Grill, A.; Avouris, P. 100-GHz Transistors from Wafer-Scale Epitaxial Graphene. *Science* **2010**, *327*, 662–662.
- Zhang, Y. B.; Tang, T. T.; Girit, C.; Hao, Z.; Martin, M. C.; Zettl, A.; Crommie, M. F.; Shen, Y. R.; Wang, F. Direct Observation of a Widely Tunable Bandgap in Bilayer Graphene. *Nature* **2009**, *459*, 820–823.
- Xia, F. N.; Farmer, D. B.; Lin, Y. M.; Avouris, P. Graphene Field-Effect Transistors with High On/Off Current Ratio and Large Transport Band Gap at Room Temperature. *Nano Lett.* **2010**, *10*, 715–718.
- Kang, S. J.; Kocabas, C.; Ozel, T.; Shim, M.; Pimparkar, N.; Alam, M. A.; Rotkin, S. V.; Rogers, J. A. High-Performance Electronics Using Dense, Perfectly Aligned Arrays of Single-Walled Carbon Nanotubes. *Nat. Nanotechnol.* **2007**, *2*, 230–236.
- Avouris, P. Carbon Nanotube Electronics and Photonics. *Phys. Today* **2009**, *62*, 34–40.
- Liu, J.; Hersam, M. C. Recent Developments in Carbon Nanotube Sorting and Selective Growth. *MRS Bull.* **2010**, *35*, 315–321.
- Appenzeller, J.; Knoch, J.; Derycke, V.; Martel, R.; Wind, S.; Avouris, P. Field-Modulated Carrier Transport in Carbon Nanotube Transistors. *Phys. Rev. Lett.* **2002**, *89*, 126801.
- Heinze, S.; Tersoff, J.; Martel, R.; Derycke, V.; Appenzeller, J.; Avouris, P. Carbon Nanotubes As Schottky Barrier Transistors. *Phys. Rev. Lett.* **2002**, *89*, 106801.
- Javey, A.; Guo, J.; Farmer, D. B.; Wang, Q.; Wang, D. W.; Gordon, R. G.; Lundstrom, M.; Dai, H. J. Carbon Nanotube Field-Effect Transistors with Integrated Ohmic Contacts and High-K Gate Dielectrics. *Nano Lett.* **2004**, *4*, 447–450.
- Palacios, J. J.; Tarakeshwar, P.; Kim, D. M. Metal Contacts in Carbon Nanotube Field-Effect Transistors: Beyond The Schottky Barrier Paradigm. *Phys. Rev. B* **2008**, *77*, 113403.
- Andriotis, A. N.; Menon, M. Structural and Conducting Properties of Metal Carbon-Nanotube Contacts: Extended Molecule Approximation. *Phys. Rev. B* **2007**, *76*, 045412.
- Kim, K. S.; Zhao, Y.; Jang, H.; Lee, S. Y.; Kim, J. M.; Ahn, J. H.; Kim, P.; Choi, J. Y.; Hong, B. H. Large-Scale Pattern Growth of Graphene Films for Stretchable Transparent Electrodes. *Nature* **2009**, *457*, 706–710.
- Bae, S.; Kim, H.; Lee, Y.; Xu, X. F.; Park, J. S.; Zheng, Y.; Balakrishnan, J.; Lei, T.; Kim, H. R.; Song, Y. I. Roll-To-Roll Production of 30-Inch Graphene Films for Transparent Electrodes. *Nat. Nanotechnol.* **2010**, *5*, 574–578.
- Son, Y. W.; Cohen, M. L.; Louie, S. G. Energy Gaps in Graphene Nanoribbons. *Phys. Rev. Lett.* **2006**, *97*, 216803.
- Ritter, K. A.; Lyding, J. W. The Influence of Edge Structure on the Electronic Properties of Graphene Quantum Dots and Nanoribbons. *Nat. Mater.* **2009**, *8*, 235–242.
- Girit, C. O.; Meyer, J. C.; Erni, R.; Rossell, M. D.; Kisielowski, C.; Yang, L.; Park, C. H.; Crommie, M. F.; Cohen, M. L.; Louie, S. G.; *et al.* Graphene at the Edge: Stability and Dynamics. *Science* **2009**, *323*, 1705–1708.
- Qi, L.; Huang, J. Y.; Feng, J.; Li, J. In Situ Observations of the Nucleation and Growth of Atomically Sharp Graphene Bilayer Edges. *Carbon* **2010**, *48*, 2354–2360.
- Lee, G.; Cho, K. Electronic Structures of Zigzag Graphene Nanoribbons with Edge Hydrogenation and Oxidation. *Phys. Rev. B* **2009**, *79*, 165440.
- Saffarzadeh, A. Modeling of Gas Adsorption on Graphene Nanoribbons. *J. Appl. Phys.* **2010**, *107*, 3409870.
- Li, T. C.; Lu, S. P. Quantum Conductance of Graphene Nanoribbons with Edge Defects. *Phys. Rev. B* **2008**, *77*, 085408.
- Shenoy, V. B.; Reddy, C. D.; Ramasubramaniam, A.; Zhang, Y. W. Edge-Stress-Induced Warping of Graphene Sheets and Nanoribbons. *Phys. Rev. Lett.* **2008**, *101*, 245501.
- Ohta, T.; Bostwick, A.; Seyller, T.; Horn, K.; Rotenberg, E. Controlling the Electronic Structure of Bilayer Graphene. *Science* **2006**, *313*, 951–954.
- Oostinga, J. B.; Heersche, H. B.; Liu, X. L.; Morpurgo, A. F.; Vandersypen, L. M. K. Gate-Induced Insulating State in Bilayer Graphene Devices. *Nat. Mater.* **2008**, *7*, 151–157.
- Liu, Z.; Suenaga, K.; Harris, P. J. F.; Iijima, S. Open and Closed Edges of Graphene Layers. *Phys. Rev. Lett.* **2009**, *102*, 015501.
- Huang, J. Y.; Ding, F.; Yakobson, B. I.; Lu, P.; Qi, L.; Li, J. In Situ Observation of Graphene Sublimation and Multi-Layer Edge Reconstructions. *Proc. Natl. Acad. Sci. U. S. A.* **2009**, *106*, 10103–10108.
- Feng, J.; Qi, L.; Huang, J. Y.; Li, J. Geometric and Electronic Structure of Graphene Bilayer Edges. *Phys. Rev. B* **2009**, *80*, 165407.
- Ebbesen, T. W.; Hiura, H. Graphene in 3-Dimensions: Towards Graphite Origami. *Adv. Mater.* **1995**, *7*, 582–586.
- Du, A. J.; Smith, S. C.; Lu, G. Q. Formation of Single-Walled Carbon Nanotube via The Interaction of Graphene Nanoribbons: Ab Initio Density Functional Calculations. *Nano Lett.* **2007**, *7*, 3349–3354.
- Koskinen, P.; Malola, S.; Hakkinen, H. Self-Passivating Edge Reconstructions of Graphene. *Phys. Rev. Lett.* **2008**, *101*, 115502.
- Ci, L.; Xu, Z. P.; Wang, L. L.; Gao, W.; Ding, F.; Kelly, K. F.; Yakobson, B. I.; Ajayan, P. M. Controlled Nanocutting of Graphene. *Nano Res.* **2008**, *1*, 116–122.
- Kotakoski, J.; Krashennnikov, A. V.; Nordlund, K. Energetics, Structure, and Long-Range Interaction of Vacancy-Type Defects in Carbon Nanotubes: Atomistic Simulations. *Phys. Rev. B* **2006**, *74*, 245420.

39. He, Y.; Zhang, C.; Cao, C.; Cheng, H. P. Effects of Strain and Defects on the Electron Conductance of Metallic Carbon Nanotubes. *Phys. Rev. B* **2007**, *75*, 235429.
40. Chico, L.; Crespi, V. H.; Benedict, L. X.; Louie, S. G.; Cohen, M. L. Pure Carbon Nanoscale Devices: Nanotube Heterojunctions. *Phys. Rev. Lett.* **1996**, *76*, 971–974.
41. Orlikowski, D.; Buongiorno Nardelli, M.; Bernholc, J.; Roland, C. Theoretical STM Signatures and Transport Properties of Native Defects in Carbon Nanotubes. *Phys. Rev. B* **2000**, *61*, 14194–14203.
42. Andriotis, A. N.; Menon, M.; Srivastava, A. Transfer Matrix Approach to Quantum Conductivity Calculations in Single-Wall Carbon Nanotubes. *J. Chem. Phys.* **2002**, *117*, 2836–2843.
43. Stuart, S. J.; Tutein, A. B.; Harrison, J. A. A Reactive Potential for Hydrocarbons with Intermolecular Interactions. *J. Chem. Phys.* **2000**, *112*, 6472–6486.
44. Brandbyge, M.; Mozos, J. L.; Ordejon, P.; Taylor, J.; Stokbro, K. Density-Functional Method for Nonequilibrium Electron Transport. *Phys. Rev. B* **2002**, *65*, 165401.
45. Soler, J. M.; Artacho, E.; Gale, J. D.; Garcia, A.; Junquera, J.; Ordejon, P.; Sanchez-Portal, D. The SIESTA Method for Ab Initio Order-N Materials Simulation. *J. Phys.: Condens. Matter* **2002**, *14*, 2745–2779.
46. Troullier, N.; Martins, J. L. Efficient Pseudopotentials for Plane-Wave Calculations. *Phys. Rev. B* **1991**, *43*, 1993–2006.
47. Perdew, J. P.; Zunger, A. Self-Interaction Correction to Density-Functional Approximations for Many-Electron Systems. *Phys. Rev. B* **1981**, *23*, 5048–5079.